Chemical Engineering Journal 397 (2020) 125472

Contents lists available at ScienceDirect

Chemical Engineering Journal

journal homepage: www.elsevier.com/locate/cej

Exploring the usage of $LiCrTiO_4$ as cathode towards constructing 1.4 V class Li-ion cells with graphite anode recovered from spent Li-Ion battery

Krishnan Subramanyan[a], Subramanian Natarajan[a], Yun-Sung Lee[b,*], Vanchiappan Aravindan[a,*]

[a] Department of Chemistry, Indian Institute of Science Education and Research (IISER), Tirupati 517507, India
[b] Department of Advanced Chemicals and Engineering, Chonnam National University, Gwang-ju 61186, Republic of Korea

HIGHLIGHTS

- 1.4 V class "Rocking –chair" type Li-ion cells are fabricated with $LiCrTiO_4$ cathode.
- Ti^{4+} to T^{3+} couple is used for the reversible intercalation of Li-ions.
- Graphite anode is recovered from the spent Li-ion battery.
- Prior to the fabrication of Li-ion cells, the anode is electrochemically lithiated (LiC_6).
- The $LiCrTiO_4/LiC_6$ showed a maximum energy density of 103 Wh kg^{-1}.

GRAPHICAL ABSTRACT

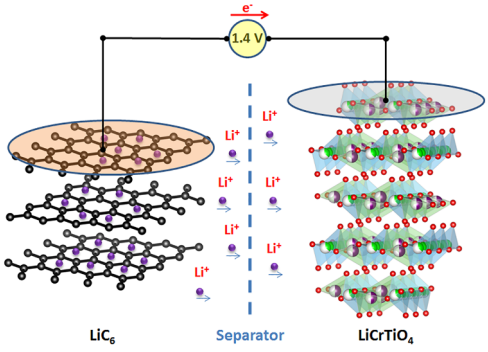

ARTICLE INFO

Keywords:
Li-ion battery
Rocking-chair
Spinel
Graphite
Recycling

ABSTRACT

Titanium-based spinel anodes had always been a favourite for lithium-ion batteries owing to their excellent stability, safety, and ease of fabrication. $LiCrTiO_4$, with all the benefits of the spinel structure, has enhanced benefits such as better electronic conductivity owing to the presence of chromium. It is an excellent candidate as an electrode for Li-ion batteries and the as-prepared material displays an initial reversible capacity of ~150 mAh g^{-1} at 0.1 A g^{-1}. This material is then used as a cathode for a Li-ion full-cell with an electrochemically pre-lithiated graphitic anode (LiC_6), recovered from spent Li-ion batteries, to form a 1.4 V rocking chair battery. The full-cell exhibited an energy density as high as 103 Wh kg^{-1} and maintaining excellent cycling stability for over 200 cycles. An *in-situ* impedance study of $LiCrTiO_4$ was done along with the temperature testing of the full-cell.

1. Introduction

The euphoria followed by the industrial revolution was far gone when the exigency of global warming rose caused by the inordinate usage of fossil fuels, which in turn drove the society to use non-CO_2 evolving energy technologies. Li-ion batteries clearly won over all other battery technologies with their high energy density, light-weight, and their amenity with portable as well as stationary electronic equipment [1–4]. The "shuttle-cock" model Li-ion batteries with intercalation based layered transition metal oxide cathode $LiCoO_2$ was the first one to be commercialized [5], followed by other transition metal oxides structures such as spinel, and olivine [6]. Besides graphite, Ti-based spinel compounds such as $Li_4Ti_5O_{12}$ (LTO) gained popularity as anode owing to its immense operational safety (a high operating voltage

* Corresponding authors.
E-mail addresses: leeys@chonnam.ac.kr (Y.-S. Lee), aravindan@iisertirupati.ac.in (V. Aravindan).

https://doi.org/10.1016/j.cej.2020.125472
Received 17 March 2020; Received in revised form 30 April 2020; Accepted 11 May 2020
Available online 13 May 2020
1385-8947/

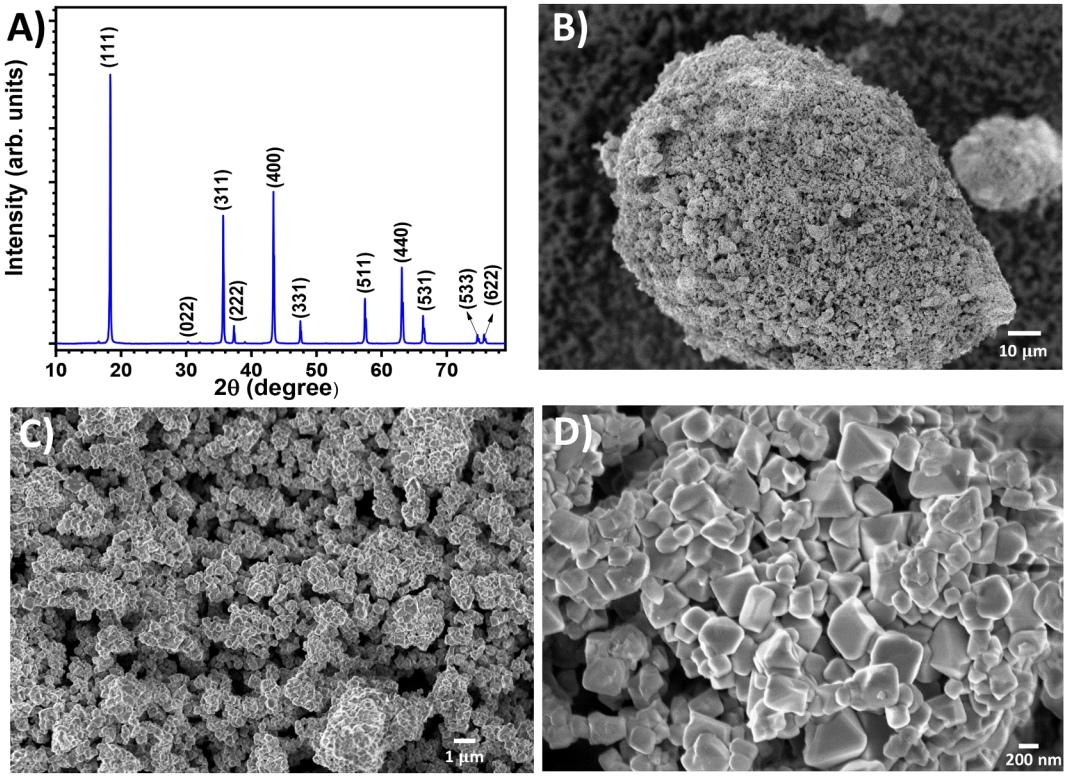

Fig. 1. (A) The powder XRD patterns of the synthesized $LiCrTiO_4$, (B-D) SEM images of $LiCrTiO_4$ with various magnifications.

~1.55 V *vs.* Li which prevents lithium plating), ease of synthesis, scalability, and its "zero-strain" nature [7–10]. An insulating nature of the delithiated LTO severely limits its high and low-temperature performances [11,12]. Also, LTO has been found to exhibit reduced diffusion coefficient ($<10^{-6}$ cm^2 s^{-1}) and poor electronic conductivity ($<10^{-13}$ S cm^{-1}), leading to poor high power performance [13]. Even though by introducing carbon, the conductivity can be enhanced, but this can lead to a problem of dilution of volumetric capacity [14]. The lithiated spinal, $LiCrTiO_4$ formed through replacing one Li^+ and two Ti^{4+} with three Cr^{3+} in LTO, can provide an almost "zero-strain" material with very negligible volume expansion (~0.7%), a flat discharge plateau at a potential ~1.5 V *vs.* Li, better rate performance and its ease of scalability for bulk industrial production [15–20]. Additionally, the inclusion of Cr^{3+} ions by replacing Ti^{4+} improves the electrical conductivity, which can provide improved high rate performance [21]. In pristine LTO, an energy gap of 2.3 eV exists between the filled O 2p valence band and the Ti 3d conduction band, making it a poor electronic conductor. The improved electrical conductivity of $LiCrTiO_4$ can be explained by the fact that doping Cr^{3+} into LTO introduces Cr 3d bands which are very close to the Ti 3d bands, which promotes the excitation of electrons from the former to the latter [22].

Here, we have formed a high performance 1.4 V "rocking-chair" model full-cell with a graphite anode (recovered from spent Li-ion batteries), with lab synthesized bare $LiCrTiO_4$. This full-cell is an excellent alternative for the conventional Pb-acid, Ni-MH, and Ni-Cd batteries for low-voltage miniature applications, which can mitigate the problem of limited cobalt and nickel resources [23]. The unwanted memory loss of Ni-MH and Ni-Cd batteries can be avoided, as well as the toxicity of lead, nickel, and cadmium poses a real threat during the use as well as the disposal of these batteries [24–27]. In $LiCrTiO_4$, chromium is present as Cr^{3+}, whose role is the structural stabilization and doesn't participate in the electrochemical performance. This trivalent form of chromium is not dangerous, rather the hexavalent form is acutely toxic, which makes $LiCrTiO_4$ safe for use [28]. Further, both the anode and cathode of this full-cell are insertion type materials with sturdy structure, which helps in the cycling stability as well as better high rate performance due to the ease of insertion and extraction. This robust nature also provides higher safety of the cell [29]. An *in-situ* impedance study of the as-synthesized $LiCrTiO_4$, as well as a temperature dependence of the full-cell, has also been performed.

2. Experimental section

2.1. Synthesis of $LiCrTiO_4$

$LiCrTiO_4$ was prepared through a conventional solid-state route where, stoichiometric ratios of commercially available Cr_2O_3 (Sigma 98%), TiO_2 (Sigma 99.8%), Li_2CO_3 (Sigma 99%) were weighed with 3% excess of lithium salt to compensate for the lithium loss during the reaction. These were mixed well-using mortar and pestle which was then pelletized and heated in a box furnace at 800 °C for 20 h at a ramp rate of 5 °C/min. The above product was naturally cooled to room temperature and was again powdered well-using mortar and pestle.

2.2. Material characterization

The structural analysis of the sample was done through XRD (Rigaku Ultima IV), whereas the composition and micro-morphology analysis was carried out through field emission scanning electron microscopy (FE-SEM, Zeiss Ultra Plus FE-SEM), high-resolution transmission electron microscopy (HR-TEM), selected area electron diffraction pattern (SAED), and energy-dispersive X-ray spectroscopy (EDS) (JEM-2000, EX-II, JEOL, JAPAN)

2.3. Electrochemical measurements

The composite electrodes were made with 10 mg of $LiCrTiO_4$, 2 mg of conductive additive (acetylene black), and 2 mg of binder (teflonized acetylene black, TAB-2) pressed on a 200 mm^2 stainless steel mesh (Goodfellow, UK), which acted as the current collector. The as-prepared

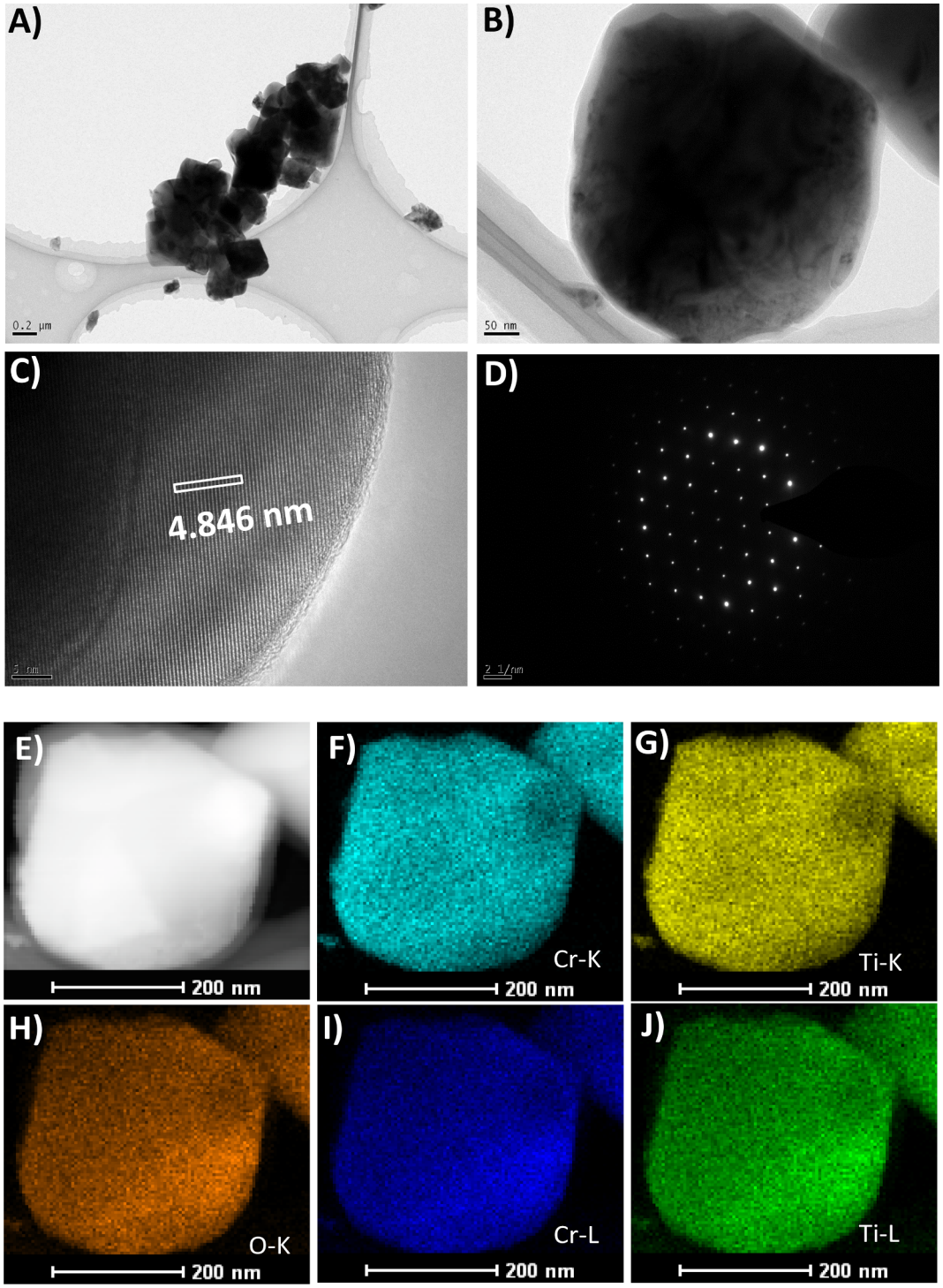

Fig. 2. (A, B) TEM images of solid-state synthesized $LiCrTiO_4$, (C) HR-TEM image, (D) SAED pattern, (E) STEM-HAADF image, and (F-J) Elemental distribution.

electrode was dried overnight at 60 ˚C in a vacuum oven, before cell assembly in an Ar-filled glove box. The CR2016 cells were made with glass microfiber separators (Whatman, cat no. 1825–047, UK) and using 1 M $LiPF_6$ in ethylene carbonate (EC): dimethyl carbonate (DMC) (1:1 vol%) as the electrolyte (Tomiyama, Japan). While recording the CV traces, lithium metal was used as both the reference as well as the counter electrode in half-cells. The anode material for full-cell was graphite recovered from spent lithium-ion battery [41], and the as-obtained graphite was heated at 700 ˚C for 2 h in the Ar atmosphere to eliminate any trace amount of organic impurities. The graphite electrodes were made by casting a slurry of the active material, conductive additive (acetylene black), and binder polyvinylidenefluoride (PVdF) (80:10:10 wt%) in N-Methyl-2-pyrrolidone (NMP, Sigma) on copper foil, which was the current collector. This was allowed to dry overnight and was then cut into 200 mm^2 electrodes. The graphite electrodes were then electrochemically pre-lithiated in a Swagelok cell assembled in an argon-filled glove box, followed by which it was re-inserted into the glove box, and the electrode was carefully removed. The balanced full-cell was constructed using this pre-lithiated graphite anode, $LiCrTiO_4$ cathode employing a polypropylene separator (Celgard- 25 μ m thickness × 85 mm width), with 1 M $LiPF_6$ in EC: DMC. The half-cell performances, full-cell performances as well as the cyclic

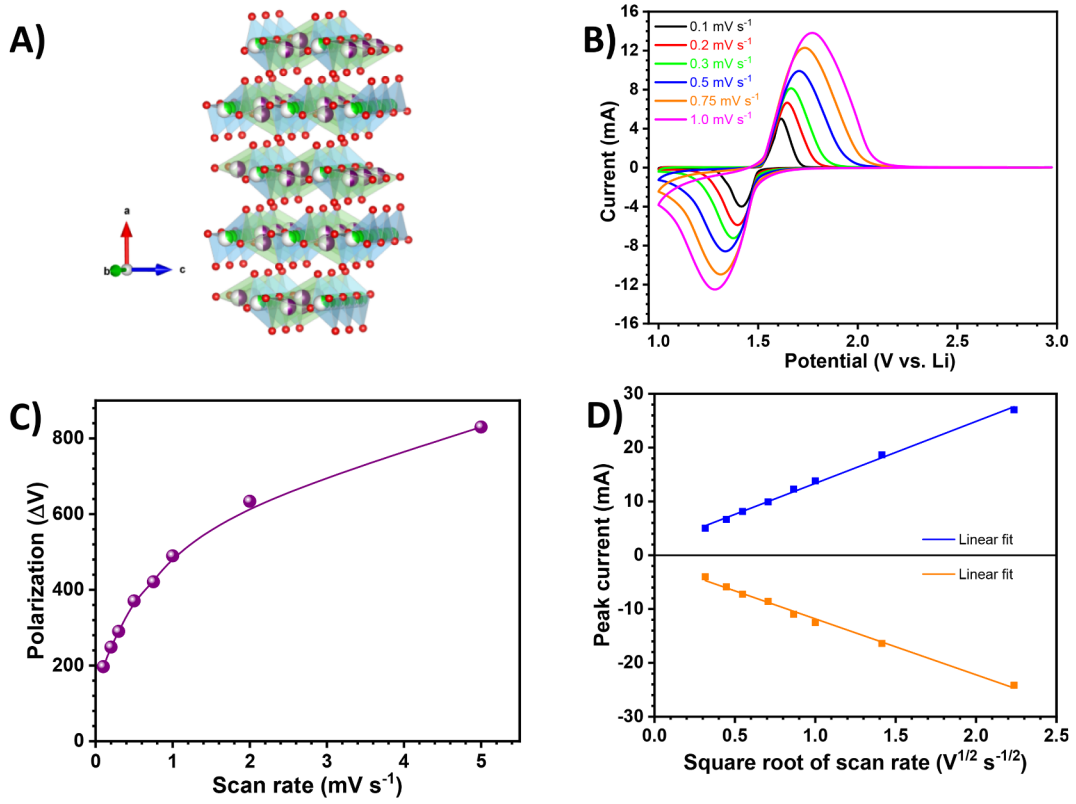

Fig. 3. (A) Crystal structure of $LiCrTiO_4$, (B) CV traces of Li/$LiCrTiO_4$ half-cells at various scan rates from 0.1 to 5.0 mV s^{-1} between 1.0 and 2.75 V in which lithium metal served as both the reference and counter electrode, (C) polarisation in the Li/$LiCrTiO_4$ half-cell with the change in the scan rate, and (D) relation between the peak current (i_p) and the square root of scan rate ($V^{1/2}$).

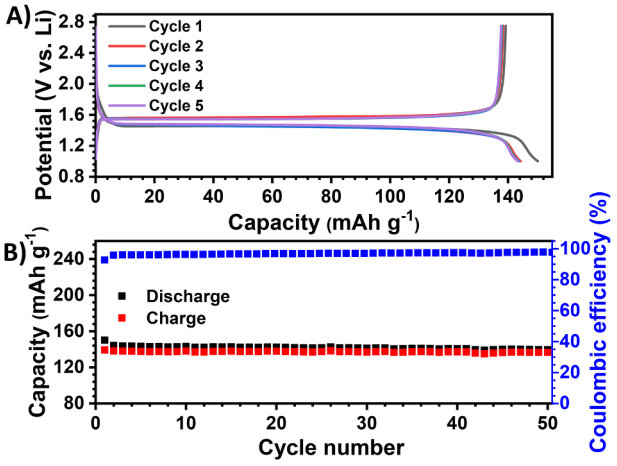

Fig. 4. (A) Galvanostatic charge–discharge curves of initial five cycles of the Li/$LiCrTiO_4$ half-cell at a current density of 100 mA g^{-1} between 1.0 and 2.75 V, and (B) cycling profile of Li/$LiCrTiO_4$ half-cell at a current density of 100 mA g^{-1} between 1.0 and 2.75 V along with Coloumbic efficiency.

voltammograms were recorded using a Bio-logic BCS series battery tester.

3. Results and discussion

The powder X-ray diffraction (XRD) pattern of the as-prepared $LiCrTiO_4$ is shown in Fig. 1a, whose peaks have been marked according to the space group, $Fd\bar{3}m$ and this matches with the previous reports [30]. Apparently, there is no secondary phase was observed. Further, the sharp and prominent reflections signify the highly crystalline nature of the spinel phase prepared by the solid-state route. The scanning electron microscopy (SEM) images denote the uniform distribution of particle size (*i.e.* sub-micron), with lesser particle agglomeration, which can promote the performance of the electrode.

Fig. 2a and b show the transmission electron microscope (TEM) image of the $LiCrTiO_4$ synthesized with particle size in the order of few hundreds of nanometers. The high-resolution TEM (HR-TEM) image in Fig. 2c shows the long-range order of the prepared material, which shows its regularity and periodicity proving the excellent crystallinity of the material. The selected area electron diffraction (SAED) pattern in Fig. 2d has regularly spaced diffraction rings confirming the crystallinity of the material synthesized and parallels the XRD measurement. The high-angle annular dark-field scanning tunneling electron microscopy (STEM-HAADF) image is shown in Fig. 2e with the elemental mapping given in Fig. 2f–j which shows the presence of Li, Cr, Ti, and O with very uniform distribution. The close and uniform distribution helps in the promotion of electron transportation.

3.1. Half-cell performance

The crystal structure of $LiCrTiO_4$ belongs to that of a normal spinel AB_2O_4 with $Fd\bar{3}m$ group symmetry, where the Li occupies the tetrahedral 8(a) sites, whereas B (Cr and Ti) occupies the octahedral 16(d) sites with 6 oxygen atoms surrounding them in a cubic closed packing. This eventually facilitates the three-dimensional Li-ion pathways for the reversible accommodation of Li-ion. Fig. 3b shows the cyclic voltammogram (CV) traces of Li/$LiCrTiO_4$ half-cell, in which lithium metal serves as both the counter and reference electrode, and recorded between 1.0 and 2.75 V *vs.* Li at different scan rates from 0.1 to 5.0 mV s^{-1}. As the scan rate increases, the current increases and a significant increase in the polarization can also be observed, which is evident in Fig. 3c. This is expected, since the higher rates, the complete

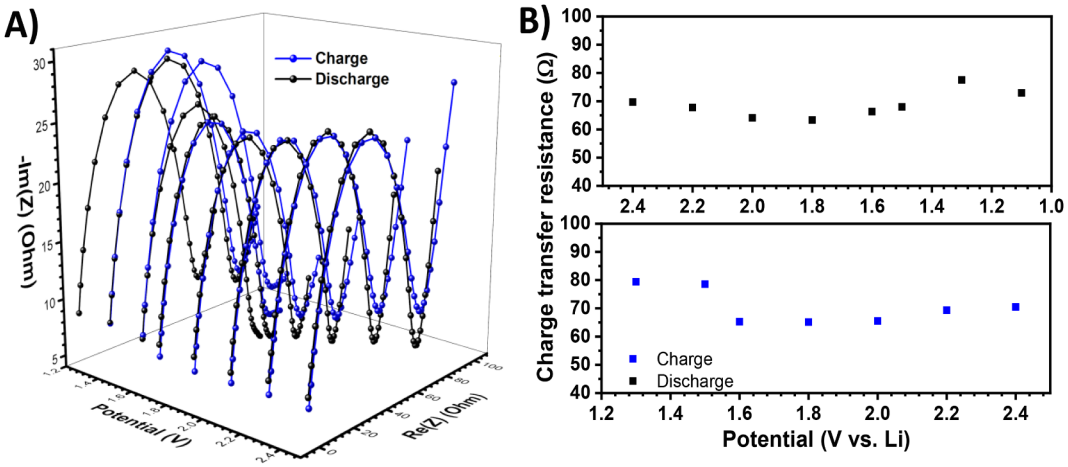

Fig. 5. (A) *In-situ* Impedance study of the Li/LiCrTiO$_4$ half-cell at different potentials during charge and discharge, and (B) charge transfer resistance at various potentials during charge and discharge of the Li/LiCrTiO$_4$ half-cell.

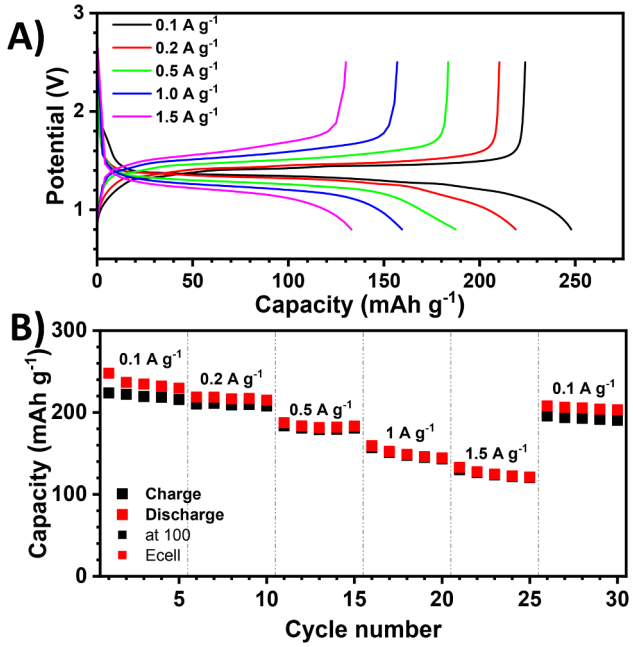

Fig. 6. (A) Galvanostatic charge–discharge curves of rate performance of the pre-lithiated recovered graphite/LiCrTiO$_4$ full-cell at 0.1, 0.2, 0.5, 1.0, and 1.5 A g^{-1} between 0.8 and 2.5 V, and (B) capacity value of the full-cell at various current density values for five cycles/current density.

participation of the active material is limited. The Li$^+$ insertion into the LiCrTiO$_4$ takes place around 1.4 V *vs.* Li, which is denoted by the reduction of Ti^{4+} to Ti^{3+}, which can be observed at lower scan rates. The oxidation of Ti^{3+} to Ti^{4+} denotes the de-insertion of Li$^+$ and is indicated by the sharp peak at ~1.6 V *vs.* Li. The insertion-disinsertion of Li$^+$ into LiCrTiO$_4$ can be represented as below.

$$LiCrTiO_4 + Li^+ + e^- \rightleftharpoons Li_2CrTiO_4$$

Using the data obtained from the CV, the diffusion coefficient of Li$^+$ at various scan rates were calculated through the Randles-Sevcik equation, which is given as (at room temperature, 25 °C):

$$i_p = 2.69 \times 10^5 n^{3/2} A C_0 D^{1/2} V^{1/2}$$

where i_p is the peak current recorded in the CV in mA, n is the number of electrons transferred during the redox reaction, A is the electrode area in cm^2, D is the diffusion coefficient in cm^2 s^{-1}, V is the scan rate in mV s^{-1}. A plot with a square of scan rate *vs.* peak current is shown in Fig. 3d., whose slope was used to calculate the diffusion coefficient for Li$^+$ ion during oxidation and reduction process which was found to be ~ $4.6 \times 10^{-10}$and ~ 3.7×10^{-10}cm^2 s^{-1}, respectively. The obtained diffusion coefficient values are much higher than those observed for LTO [31] and are similar to the result obtained in previously performed studies on LiCrTiO$_4$ [16]. The as-synthesized LiCrTiO$_4$ has a higher Li$^+$ diffusion coefficient, which hints the material has higher mobility for Li$^+$ ions, which can revamp the performance at higher current rates.

Fig. 4a shows the initial 5 cycles of the Li/LiCrTiO$_4$ half-cell at a high current density of 100 mA g^{-1} between 1.0 and 2.75 V *vs.* Li. It can be seen that the initial discharge capacity amounted to ~150 mAh g^{-1} and in the subsequent charge–discharge values amounted to ~140 mAh g^{-1} and the corresponding initial coulombic efficiency of ~93% which then increases to ~100% in the following cycles. This high initial discharge capacity and the further reduction in capacity can be accounted for formation cycle, or in other words structural re-arrangement where lithium will be irreversibly consumed. The lithium-ion insertion – de-insertion procedure is denoted by a long plateau at ~1.5 V *vs.* Li in the galvanostatic cycling, which is the classic signature of a two-phase reaction [32]. Fig. 4b gives the long-term cycling of the Li/LiCrTiO$_4$ half-cell at a high current density of 100 mA g^{-1} and after 50 cycles the half-cell displays a reversible capacity of ~140 mAh g^{-1} with coulombic efficiency reaching > 99% after a few initial cycles, showcasing excellent stability even after cycling at a high current rate.

An *in-situ* impedance study of the Li/LiCrTiO$_4$ half-cell was also performed, which is shown in Fig. 5a where the impedance of the half-cell at different voltages during charge and discharge was measured. The impedance study is performed by initially applying a high-frequency current and progressing towards lower frequencies. The responses that are observed in the high-frequency regime correspond to charge transfer processes whereas the responses in the low-frequency regime correspond to diffusion-controlled processes. The high-frequency response in an ideal case for a lithium-ion battery would be a semi-circle, with the lower *x*-axis intercept value giving the solution resistance, and the higher *x*-axis intercepts giving the sum of solution resistance and the charge transfer resistance (R_{ct}). The low-frequency region displays a 'tail' which is known as Warburg impedance which would be at an angle of 45°. With lithiation/de-lithiation, the impedance was seen to vary, but the impedance values at a particular voltage during discharge/charge remained common. The R_{ct} at each voltage was calculated during discharge/charge from the intercept of the impedance, which is shown in Fig. 5b. As expected that with lithiation, the R_{ct} decreases, and then increases.

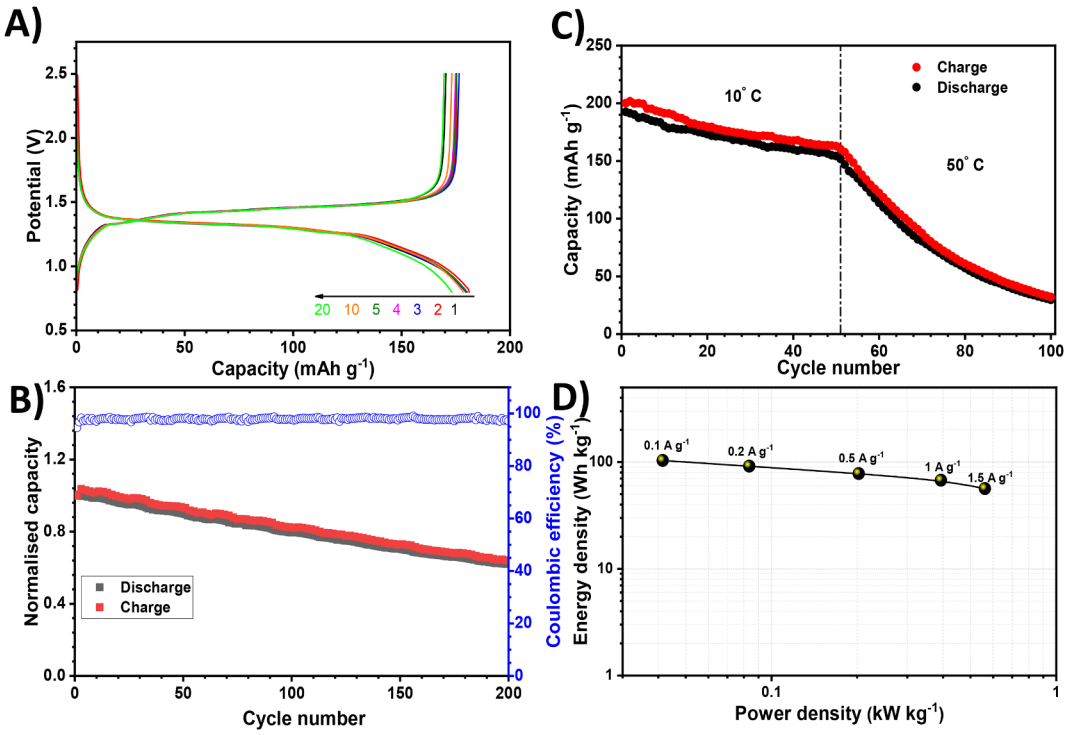

Fig. 7. (A) Galvanostatic charge–discharge curves for the full-cell from 0.8 to 2.5 V at a current density of 250 mA g^{-1}, (B) capacity values and coulombic efficiency for long-term cycling of the full-cell. Capacity and the current density have been calculated based on the anode mass loading, (C) Temperature-dependent performance of LiC_6/$LiCrTiO_4$ full-cell at 100 mA g^{-1} from 0.8 to 2.5 V at 10 °C and 50 °C, and (D) Ragone plot of the full-cell with energy and power density.

3.2. Full-cell performance

Upon the fabrication of full-cell, the capacity matching is essential to achieve high-performance Li-ion power packs. Further, though the $Cr^{3+/4+}$ redox reaction is electrochemically possible at higher potentials (~5.25 V *vs.* Li), but it is beyond the thermodynamic potential window of the traditional carbonate-based electrolyte solution [33]. Hence, we would like to utilize the $Ti^{4+/3+}$ couple by sacrificing the working potential, in which Cr^{3+} acts as only the passive compound. As stated, the optimization of the capacity of both electrodes is necessary. Accordingly, galvanostatic charge–discharge curves of the graphite anode prepared/recovered from used Li-ion batteries at a current density of 100 mA g^{-1} from 0.005 to 2 V *vs.* Li. This approach provides a manifold advantage, *i.e.*, efficient recycling of spent Li-ion battery, no need to optimize the electrode material (since the material is already in the commercial batteries), cost-effective active material, etc. The half-cell with recovered graphite rendered the initial discharge capacity reaching ~412 mAh g^{-1} which is crossing the theoretical capacity (372 mAh g^{-1}) towards the formation of LiC_6. The charge–discharge curves as well as a cycling performance of this recovered graphite is shown in Fig. S1. This excess capacity accounted for the solid-electrolyte interphase (SEI) film formation of the graphite anode through the decomposition of the electrolyte [34]. It is worth mentioning that, there are no free Li-ions available to shuttle between the two electrodes within the confined potential window. Therefore, either one of the active material must be pre-lithiated. In the present case, by considering the large irreversibility, the recovered graphite has been electrochemically pre-lithiated (LiC_6) under the balanced mass loading conditions.

A balanced full-cell LiC_6/$LiCrTiO_4$ was constructed with an operating potential of ~1.4 V. Fig. 6 a and b represents the rate performance between 0.8 and 2.5 V of the as-constructed full-cell, where Fig. 6a gives the galvanostatic charge–discharge cycles. At a relatively low rate of 100 mA g^{-1}, the cell displayed the initial reversible capacity of ~250 mAh g^{-1}. The full-cell is subjected to different current densities going up to ultra-high rate of 1.5 A g^{-1} and even then the cell manages to maintain its capacity as it can be seen that even after such a heavy load, the cell displays ~225 mAh g^{-1} when again subjected to a current density of 100 mA g^{-1}. Even, the cell is subjected to multiple cycles at high current rates, the full-cell retains its capacity when swung back to a lower current density, which is clear from Fig. 6b. This can be attributed to the agile ion-mobility, high electronic conductivity and the robust nature of $LiCrTiO_4$ cathode.

The same full-cell was subjected to long-term cycling between 0.8 and 2.5 V at a high current rate of 250 mA g^{-1}, which managed to retain ~63% of its initial capacity after 200 cycles, which can be seen from Fig. 7 a and b. The inevitable side-reactions, especially graphitic anode can lead to the loss of lithium in an irreversible manner, which can also degrade the performance. Moreover even if the anode and cathode half-cells exhibit excellent performance with mettalic Li, their limited lithium source and poor compatability with counter electrode can result in the relatively poorer performance in full-cell configuration [35]. The full-cell was fabricated with graphite recycled from spent Li-ion battery as well as bare $LiCrTiO_4$ whose performance can be refined by improving the electrodes such as carbon coating $LiCrTiO_4$ [16], ball-milling, downsizing, etc. A Ragone plot with the power density and energy density calculated based on the total mass of the cell at various rates is shown in Fig. 7c. Accordingly, the cell delivered the maximum energy density of ~103 Wh kg^{-1}. To find the temperature dependence of the as-fabricated full-cell, a temperature study was also performed, as shown in Fig. 7d using the as-fabricated full-cell between 0.8 and 2.5 V at a current density of 100 mA g^{-1}.

At low-temperature regime (10 °C), the full-cell initially displayed a charge capacity of ~200 mAh g^{-1} which slowly degraded to ~163 mAh g^{-1} after 50 cycles. The initial capacity is lesser when compared to the room temperature full-cell, which can be majorly attributed to the sluggish Li^+ ion diffusion into graphite rather than the ionic mobility in the electrolyte or the SEI film formation [36,37]. Along with this, the increase in the internal resistance of the cell at low temperatures can also lead to degradation in performance [38]. This full-cell was then suscepted to a high temperature and was seen that at elevated

temperature (50 °C), the loss at low-temperature was not recovered when switched to 50 °C. Additionally, the capacity decay was very rapid and after 50 cycles, the full-cell managed to hold on to 20% of initial charge capacity. This loss on capacity can be accounted by a lot of factors such as thermal decomposition of the electrolyte employed as well as that of the SEI layer formed on the electrode surface, whose replication irreversibly consumes lithium [35,39,40].

4. Conclusion

$LiCrTiO_4$ synthesized through the solid-state process was analyzed as a reversible intercalation host for the accommodation of Li-ions. The as-synthesized material was shown to exhibit higher Li-ion diffusion, which points to a higher rate performance behaviour. The impedance study revealed a lesser charge-transfer resistance as well as total impedance in the voltage range 1.6–2.0 V in the charge–discharge voltage range which corresponds to the lithium insertion into $LiCrTiO_4$. A full-cell was fabricated with the pre-lithiated recovered-graphite anode (LiC_6) and $LiCrTiO_4$ cathode, which worked as a 1.4 V rocking-chair full-cell whose temperature study revealed its performance at high and low temperatures, with the higher degradation in performance at the high-temperature regime. A rate performance, as well as a galvanostatic charge–discharge study of the full-cell, was done. The performance can be further upgraded by employing methods such as ball-milling, carbon coating, etc.

Declaration of Competing Interest

The authors declare that they have no known competing financial interests or personal relationships that could have appeared to influence the work reported in this paper.

Acknowledgments

KS thanks to the Department of Science & Technology (DST), Govt. of India for the financial support through INSPIRE fellowship (IF180157). YSL acknowledges the financial support from the National Research Foundation of Korea (NRF) grant funded by the Korea government (Ministry of Science, ICT & Future Planning) (No. 2019R1A4A2001527). VA acknowledges financial support from the Science & Engineering Research Board (SERB), a statutory body of the DST, Govt. of India, through the Ramanujan Fellowship (SB/S2/RJN-088/2016).

Appendix A. Supplementary data

Supplementary data to this article can be found online at https://doi.org/10.1016/j.cej.2020.125472.

References

[1] E.J. Cairns, P. Albertus, Batteries for electric and hybrid-electric vehicles, Annu. Rev. Chem. Biomol. Eng. 1 (2010) 299–320, https://doi.org/10.1146/annurev-chembioeng-073009-100942.
[2] D. Larcher, J.-M. Tarascon, Towards greener and more sustainable batteries for electrical energy storage, Nat. Chem. 7 (2014) 19, https://doi.org/10.1038/nchem.2085.
[3] P. Poizot, F. Dolhem, Clean energy new deal for a sustainable world: from non-CO2 generating energy sources to greener electrochemical storage devices, Energy Environ. Sci. 4 (2011) 2003–2019, https://doi.org/10.1039/C0EE00731E.
[4] J.-M. Tarascon, M. Armand, Issues and challenges facing rechargeable lithium batteries, Nature 414 (2001) 359–367, https://doi.org/10.1038/35104644.
[5] K. Mizushima, P.C. Jones, P.J. Wiseman, J.B. Goodenough, LixCoO2 (0<x<-1): A new cathode material for batteries of high energy density, Mater. Res. Bull. 15 (1980) 783–789, https://doi.org/10.1016/0025-5408(80)90012-4.
[6] N. Nitta, F. Wu, J.T. Lee, G. Yushin, Li-ion battery materials: present and future, Biochem. Pharmacol. 18 (2015) 252–264, https://doi.org/10.1016/j.mattod.2014.10.040.
[7] S. Jayaraman, V. Aravindan, N. Shubha, M. Ulaganathan, S. Madhavi, Exploring anatase TiO2 nanofibers as new cathode for constructing 1.6 V class, "Rocking-Chair" type li-ion cells, Part. Part. Syst. Char. 33 (2016) 306–310, https://doi.org/10.1002/ppsc.201600044.
[8] X. Sun, P.V. Radovanovic, B. Cui, Advances in spinel Li4Ti5O12 anode materials for lithium-ion batteries, New J. Chem. 39 (2015) 38–63, https://doi.org/10.1039/C4NJ01390E.
[9] K. Zaghib, M. Simoneau, M. Armand, M. Gauthier, Electrochemical study of Li4Ti5O12 as negative electrode for Li-ion polymer rechargeable batteries, J. Power Sources 81–82 (1999) 300–305, https://doi.org/10.1016/S0378-7753(99)00209-8.
[10] T. Ohzuku, A. Ueda, N. Yamamoto, Zero-strain insertion material of Li [Li1/3Ti5/3] O4 for rechargeable lithium cells, J. Electrochem. Soc. 142 (1995) 1431–1435, https://doi.org/10.1149/1.2048592.
[11] C.Y. Ouyang, Z.Y. Zhong, M.S. Lei, Ab initio studies of structural and electronic properties of Li4Ti5O12 spinel, Electrochem. Commun. 9 (2007) 1107–1112, https://doi.org/10.1016/j.elecom.2007.01.013.
[12] T. Brousse, P. Fragnaud, R. Marchand, D.M. Schleich, O. Bohnke, K. West, All oxide solid-state lithium-ion cells, J. Power Sources 68 (1997) 412–415, https://doi.org/10.1016/S0378-7753(97)02521-4.
[13] R. Agrawal, C. Chen, S. Dages, C. Wang, Lithium-ion capacitor based on electrodes constructed via electrostatic spray deposition, ECS Trans. 72 (2016) 45–53, https://doi.org/10.1149/07208.0045ecst.
[14] V. Aravindan, K. Karthikeyan, K.S. Kang, W.S. Yoon, W.S. Kim, Y.S. Lee, Influence of carbon towards improved lithium storage properties of Li2MnSiO4 cathodes, J. Mater. Chem. 21 (2011) 2470–2475, https://doi.org/10.1039/C0JM03471A.
[15] X. Feng, C. Shen, N. Ding, C. Chen, Lithium chromium oxide modified spinel LiCrTiO4 with improved electrochemical properties, J. Mater. Chem. 22 (2012) 20861–20865, https://doi.org/10.1039/C2JM32673F.
[16] J. Yang, B. Yan, J. Ye, X. Li, Y. Liu, H. You, Carbon-coated LiCrTiO4 electrode material promoting phase transition to reduce asymmetric polarization for lithium-ion batteries, PCCP 16 (2014) 2882–2891, https://doi.org/10.1039/c3cp54399d.
[17] V. Aravindan, W.C. Ling, S. Madhavi, LiCrTiO4: a high-performance insertion anode for lithium-ion batteries, ChemPhysChem 13 (2012) 3263–3266, https://doi.org/10.1002/cphc.201200398.
[18] C. Lv, X. Zhao, Y. Zhu, Y. Xia, D. Yang, 20,000 ligands under the sea: metal-organic supramolecules from the ocean, Matter. 2 (2020) 10–12, https://doi.org/10.1016/j.matt.2019.12.005.
[19] C. Lv, H. Liu, D. Li, S. Chen, H. Zhang, X. She, X. Guo, D. Yang, Ultrafine FeSe nanoparticles embedded into 3D carbon nanofiber aerogels with FeSe/Carbon interface for efficient and long-life sodium storage, Carbon N. Y. 143 (2019) 106–115, https://doi.org/10.1016/j.carbon.2018.10.091.
[20] C. Lv, W. Xu, H. Liu, L. Zhang, S. Chen, X. Yang, X. Xu, D. Yang, 3D sulfur and nitrogen codoped carbon nanofiber aerogels with optimized electronic structure and enlarged interlayer spacing boost potassium-ion storage, Small 15 (2019) 1900816, https://doi.org/10.1002/smll.201900816.
[21] Y. Yao, L. Zhang, X. Bie, H. Chen, C. Wang, F. Du, G. Chen, Exploration of spinel LiCrTiO4 as cathode material for rechargeable Mg-Li hybrid batteries, Chem. – A Eur. J. 23 (2017) 17935–17939, https://doi.org/10.1002/chem.201702075.
[22] D. Liu, C. Ouyang, J. Shu, J. Jiang, Z. Wang, L. Chen, Theoretical study of cation doping effect on the electronic conductivity of Li4Ti5O12, Phys. Status Solidi. 243 (2006) 1835–1841, https://doi.org/10.1002/pssb.200541404.
[23] U.S. Geological Survey, Mineral Commodity Summaries 2019, 2019. https://doi.org/https://doi.org/10.3133/70202434.
[24] K.K. Das, R.R. Chandramouli, B.I. B, D. Swastika, B. Shrilaxmi, M. Lata, K.J. P, B.M. S, Primary concept of nickel toxicity – an overview, J. Basic Clin. Physiol. Pharmacol. 30 (2019) 141. https://doi.org/10.1515/jbcpp-2017-0171.
[25] A.L. Wani, A. Ara, J.A. Usmani, Lead toxicity: a review, Interdiscip. Toxicol. 8 (2015) 55–64, https://doi.org/10.1515/intox-2015-0009.
[26] J. Godt, F. Scheidig, C. Grosse-Siestrup, V. Esche, P. Brandenburg, A. Reich, D.A. Groneberg, The toxicity of cadmium and resulting hazards for human health, J. Occup. Med. Toxicol. 1 (2006) 22, https://doi.org/10.1186/1745-6673-1-22.
[27] P. Manimekalai, R. Harikumar, S. Raghavan, An overview of batteries for photovoltaic (PV) systems, Int. J. Comput. Appl. 82 (2013) 29–31.
[28] F. Baruthio, Toxic effects of chromium and its compounds, Biol. Trace Elem. Res. 32 (1992) 145–153, https://doi.org/10.1007/BF02784599.
[29] J. Meng, H. Guo, C. Niu, Y. Zhao, L. Xu, Q. Li, L. Mai, Advances in structure and property optimizations of battery electrode materials, Joule 1 (2017) 522–547, https://doi.org/10.1016/j.joule.2017.08.001.
[30] K. Mukai, K. Ariyoshi, T. Ohzuku, Comparative study of Li[CrTi]O4, Li[Li1/3Ti5/3] O4 and Li1/2Fe1/2[Li1/2Fe1/2Ti]O4 in non-aqueous lithium cells, J. Power Sources 146 (2005) 213–216, https://doi.org/10.1016/j.jpowsour.2005.03.019.
[31] B. Yan, M. Li, X. Li, Z. Bai, J. Yang, D. Xiong, D. Li, Novel understanding of carbothermal reduction enhancing electronic and ionic conductivity of Li4Ti5O12 anode, J. Mater. Chem. A 3 (2015) 11773–11781, https://doi.org/10.1039/c5ta00887e.
[32] T. Ohzuku, K. Tatsumi, N. Matoba, K. Sawai, Electrochemistry and structural chemistry of Li[CrTi]O4 (Fd3m) in nonaqueous lithium cells, J. Electrochem. Soc. 147 (2000) 3592–3597, https://doi.org/10.1149/1.1393944.
[33] A. Bhaskar, D. Mikhailova, N. Kiziltas-Yavuz, K. Nikolowski, S. Oswald, N.N. Bramnik, H. Ehrenberg, 3d-Transition metal doped spinels as high-voltage cathode materials for rechargeable lithium-ion batteries, Prog. Solid State Chem. 42 (2014) 128–148, https://doi.org/10.1016/j.progsolidstchem.2014.04.007.
[34] S.J. An, J. Li, C. Daniel, D. Mohanty, S. Nagpure, D.L. Wood, The state of understanding of the lithium-ion-battery graphite solid electrolyte interphase (SEI) and its relationship to formation cycling, Carbon N. Y. 105 (2016) 52–76, https://doi.org/10.1016/j.carbon.2016.04.008.
[35] J.-H. Kim, N.P.W. Pieczonka, L. Yang, Challenges and approaches for high-voltage spinel lithium-ion batteries, ChemPhysChem 15 (2014) 1940–1954, https://doi.

org/10.1002/cphc.201400052.
[36] S.S. Zhang, K. Xu, T.R. Jow, Low temperature performance of graphite electrode in Li-ion cells, Electrochim. Acta 48 (2002) 241–246, https://doi.org/10.1016/S0013-4686(02)00620-5.
[37] C.K. Huang, J.S. Sakamoto, J. Wolfenstine, S. Surampudi, The limits of low-temperature performance of Li-ion cells, J. Electrochem. Soc. 147 (2000) 2893–2896, https://doi.org/10.1149/1.1393622.
[38] D. Ouyang, Y. He, J. Weng, J. Liu, M. Chen, J. Wang, Influence of low temperature conditions on lithium-ion batteries and the application of an insulation material, RSC Adv. 9 (2019) 9053–9066, https://doi.org/10.1039/c9ra00490d.
[39] R. Spotnitz, J. Franklin, Abuse behavior of high-power, lithium-ion cells, J. Power Sources 113 (2003) 81–100, https://doi.org/10.1016/S0378-7753(02)00488-3.
[40] F. Leng, C.M. Tan, M. Pecht, Effect of temperature on the aging rate of Li ion battery operating above room temperature, Sci. Rep. 5 (2015) 12967, https://doi.org/10.1038/srep12967.
[41] S. Natarajan, D.S. Lakshmi, H.C. Bajaj, D.N. Srivastava, Recovery and utilization of graphite and polymer materials from spent lithium-ion batteries for synthesizing polymer–graphite nanocomposite thin films, J. Environ. Chem. Eng. 3 (2015) 2538–2545, https://doi.org/10.1016/j.jece.2015.09.011.